Journal of Drug Delivery Science and Technology 113 (2025) 107335

Contents lists available at ScienceDirect

Journal of Drug Delivery Science and Technology

journal homepage: www.elsevier.com/locate/jddst

Comparative cytotoxicity of biogenic and chemical silver and gold nanoparticles on normal and tumoral lung cells

Martina Leoncini [a], Chiara Ortile [a], Susanna Tinello [a], Silvia Gross [b,c], Maddalena Mognato [a,*]

[a] Department of Biology, University of Padova, Via U. Bassi 58/B, 35131, Padova, Italy
[b] Department of Chemical Sciences, University of Padova, 35131, Padova, Italy
[c] Institute for Chemical Technology and Polymer Chemistry (ITCP), Karlsruhe Institute of Technology (KIT), Germany

ARTICLE INFO

Keywords:
Silver and gold nanoparticles
Biogenic and chemical synthesis
Lung cells
Cell death

ABSTRACT

Silver (Ag) and gold (Au) nanoparticles (NPs) are largely employed in many different fields and are typically synthesized through chemical methods, involving reduction reactions, which can result in the production of hazardous compounds harmful to both human health and the environment. As a response to these concerns, there is an increasing interest in developing more environmentally friendly approaches for their synthesis. In this study, we analysed the cytotoxic response of human cells exposed to Ag and Au NPs, produced via alternative routes: the Lee-Meisel and the Turkevich chemical methods, and the biogenic method using tea extract. Ag and Au NPs were synthesized to achieve high NP concentrations and ensure the stability of the NP suspension over time. We assessed the effects of these NPs on two different lung cell lines, one normal (HBEC3-KT) and one tumoral (A549) since the cellular response to NPs may vary depending on the tumoral status of the cells.

The results evidenced a higher cytotoxicity of Ag than Au NPs, irrespective of the synthesis method and consistent with silver's reported toxic properties. At 2 μg/mL, both biogenic and chemical Ag NPs showed minimal toxicity but at 5 μg/mL and above, biogenic Ag NPs exhibited greater cytotoxicity towards normal cells compared to cancer cells, distinguishing them from their chemical counterparts. Notably, long-term clonogenic assays revealed that biogenic Ag NPs affected the proliferation ability of cancer cells at lower concentrations than chemical Ag NPs. Biogenic Au NPs maintained minimal toxicity in both normal and cancer cells, similarly to chemically synthesized NPs, even at the highest concentration tested, highlighting the high biocompatibility of Au NPs. Our results show that biogenic synthesis using the tea extract is efficient to synthesize Ag NPs with potential anticancer or antimicrobial applications and Au NPs suitable for drug delivery.

1. Introduction

Nanobiotechnology represents a cutting-edge field at the intersection of nanotechnology and biotechnology, offering unprecedented opportunities for various applications in medicine, agriculture, environmental remediation and beyond. Among the diverse nanomaterials explored, metallic nanoparticles (NPs), particularly silver and gold, have garnered significant attention due to their unique optical, electrical, and catalytic properties [1–4]. These NPs exhibit remarkable potential in biomedical imaging, drug delivery, sensing and antimicrobial applications, among others [1,5–10].

However, the conventional methods for synthesizing metal NPs often involve the use of hazardous chemicals and harsh reaction conditions, raising concerns about their adverse effects on human health and the environment [11]. Therefore, there is a growing imperative to develop greener synthesis approaches that minimize the use of toxic reagents, energy consumption, and waste generation while maintaining the desired NPs properties [6,12]. In this context, the request for environmentally benign synthesis methods for silver (Ag) and gold (Au) NPs (NPs) has become paramount. Green synthesis strategies involve the utilization of biocompatible and renewable resources such as plant, extracts, yeast, microorganism, and biopolymers as reducing, capping and stabilizing agents [6,11]. These methods offer several advantages, including cost-effectiveness and biocompatibility, while simultaneously reducing the ecological footprint associated with NPs production [1].

Considering the pressing need for sustainable solutions in nanotechnology, and in view of potential applications of these systems in biomedicine, this work aims to evaluate the cytotoxicity of Ag and Au

* Corresponding author. Department of Biology, University of Padova, Via U. Bassi 58/B, 35131, Padova, Italy.
E-mail address: maddalena.mognato@unipd.it (M. Mognato).

https://doi.org/10.1016/j.jddst.2025.107335
Received 24 April 2025; Received in revised form 22 July 2025; Accepted 28 July 2025
Available online 5 August 2025

NPs synthesized by a biogenic approach in comparison to conventional chemical methods, specifically the well-known Lee-Meisel and Turkevich approach [13–15]. In particular, the reduction of Ag^{+} and Au^{3+} species was evaluated by the two alternative routes. For the biogenic synthesis, black tea infusion was chosen as the biogenic agent due to its easy availability and its content of molecules with antioxidant, antibacterial and antiviral activities represented by polyphenols [16,17] The biogenic syntheses were optimized to obtain high NPs concentrations and to ensure the stability of the NPs suspensions over time. The chemical synthesis was performed following two well-known protocols: The Lee-Meisel method for Ag NPs and the Turkevich one for Au NPs [14,15]. We compared the two-synthesis different approaches and evaluated any differences from both chemical and biological perspectives. Considering the possible Ag NPs and Au NPs application in the biomedical field we analysed and compared the cytotoxicity of biogenically and chemically synthesized NPs in human cells of the respiratory tract [18].

2. Materials and methods

2.1. Chemical synthesis of colloidal silver and gold NPs

The reagents we used were silver nitrate ($AgNO_3$ from Sigma-Aldrich) and tetra chloroauric acid ($HAuCl_4$) as a precursor salt and trisodium citrate ($C_6H_5Na_3O_7 \bullet 2H_2O$ from Sigma-Aldrich) as reducing and capping agent. The colloidal silver and gold NPs were prepared through the chemical reduction methods respectively described by Lee and Meisel [14] and Turkevich [15]. All the reagent solutions were prepared with Milli-Q deionized water. For NPs synthesis, 100 mL of 2.5 mM $AgNO_3$ and 100 mL of 2.5 mM $HAuCl_4$ were each heated, separately, in a beaker. When the temperature was close to the boiling point, to each solution, 10 mL of 1 % $C_6H_5Na_3O_7$ were carefully added drop by drop. The process was carried on applying a vigorous stirring to ensure the increased interaction of the reagents. The reactions were stopped once the colour change was observed, from colourless to light yellow for Ag NPs suspension and to dark red for Au NPs suspension. The reduced silver (Ag^0) and gold (Au^0) form, both, Ag NPs and Au NPs with citrate attached to the surface and dispersed in aqueous medium [19] form the colloidal suspension; these were studied from the viewpoint of physical characteristics and biological effects.

2.2. Biogenic synthesis of colloidal silver and gold NPs

We used black tea leaves (Lipton, Yellow Label) as reducing and capping agent. All the reagents solutions were prepared with Milli-Q deionized water. Black tea infusion was obtained by infusion for 15 min at room temperature (RT) of black tea leaves (1.75 g) in 300 mL Milli-Q deionized water and subsequent gravity filtration. Filtration was performed using Macherey-Nagel filter paper with a pore size of 16 μm. For NPs synthesis, 100 mL of 2.5 mM of $AgNO_3$ and of $HAucl_4$ were dissolved, separately, in a beaker. Biogenic colloidal Ag was obtained at RT by adding to 100 mL of $AgNO_3$ salt precursor 10 mL of black tea drop by drop. Unlike the biogenic synthesis of Ag NPs, the biogenic Au NPs occurred at 40 °C: once the temperature reached 40 °C, an additional 100 mL of tea infusion was added drop by drop to the 100 mL of precursor salt. Both syntheses were interrupted once the colour change to yellow-brown and dark-red occurred, respectively, for the Ag and Au NPs.

2.3. UV–Vis

UV–Vis spectroscopy was employed to analyze the optical properties of Ag NPs and Au NPs, revealing characteristic absorption peaks giving an idea about NPs formation, size, and shape. The UV–Vis spectroscopy measurement was performed using an Agilent Varian Cary 50 UV–Vis spectrophotometer (Department of Chemistry, University of Padua) in the range of 300–900 nm, using glass cuvettes.

2.4. Transmission electron microscopy

Transmission electron microscopy (TEM) analyses were performed using the FEI Tecnai G2 microscope (FEI Company, Hillsboro, OR, USA), operating at 100 kV and equipped with a side-mounted camera Olympus Veleta and a bottom-mounted camera TVIPS F114. For this analysis, a drop of each NP suspension (~1 mg/mL) was deposited onto standard carbon-coated copper grids (200-mesh) and dimensional analysis of NPs from TEM images was performed by using the Image J software.

2.5. Dynamic Light Scattering

Dynamic light scattering (DLS) was utilized to determine NPs hydrodynamic diameters in solution, providing insights into their stability and aggregation behavior. These measurements were conducted at the Department of Chemistry, University of Padua, using the DLS Zetasizer Nano S instrument (Malvern Panalytical). The same instrument has been utilized to determine Zeta Potential of the colloidal suspension which measure the surface charge indicating the suspension stability. Hydrodynamic particle diameters were obtained from cumulant fit of the autocorrelation functions at 178° scattering angle. Size measurements were performed at 37 °C. DLS measurements were performed in phosphate buffered saline (PBS) solution and in cell culture medium, with or without 3 % of fetal bovine serum (FBS), because the electric double layer produced by the highly negative surface charge of the NPs hampers reliable measurements in pure water.

2.6. Cell lines

The experiments were performed using two different human cell lines derived from the respiratory tract, normal hTERT-immortalized epithelial cells from bronchus (HBEC3-KT, ATCC® n. CRL-4051™) and alveolar type 2 lung adenocarcinoma cells (A549, ATCC CCL-185™). The morphology of these cell lines is adherent, and the doubling time is 20 h for HBEC3-KT and 24 h for A549. HBEC3-KT cells were cultured in PneumaCult™-Ex Plus Medium supplemented with Hydrocortisone Stock Solution (STEMCELL Technologies, Canada). The A549 cells were cultured in Ham's F12-K Nutrient Mixture (Life Technologies, ThermoFisher Scientific, Waltham, MA, USA) supplemented with 10 % heat-inactivated FBS (Gibco, ThermoFisher Scientific, Waltham, MA, USA) and antibiotics (38 units/mL streptomycin; 100 units/mL penicillin G, Life Technologies, ThermoFisher Scientific, Waltham, MA, USA). For cell growth in 2D, the cells were grown in T75 cm^2 flasks (FALCON) maintained at 37 °C in a humidified atmosphere of 95 % air and 5 % CO_2 and properly sub-cultured to maintain the exponential growth. For cell growth in 3D, A549 and HBEC3-KT cells were seeded in complete medium in low attachment spheroid culture plates (Nunclon™ Sphera™ 96-Well ThermoFisher Scientific, Waltham, MA, USA) and cultured for 7–9 days.

2.7. Cell treatments with silver and gold NPs

Cells were properly seeded in culture dishes in complete culture medium and 24 h later were incubated with suspensions of chemically and biogenically synthesized Ag and Au NPs. Immediately before use, the NP suspensions were sonicated for 10 min using a tip Q125 Sonicator® ultrasonic processor (QSONICA SONICATORS, Newtown, Connecticut, USA), and sterilized by filtration with 0.22 μM. The desired NP concentrations were achieved by diluting stock solutions in PneumaCult™-Ex Plus Medium (serum-free), supplemented with Hydrocortisone Stock Solution for HBEC3-KT cells, and in F12k medium with 3 % FBS for A549 cells. The low concentration of serum counteracts particle aggregation driven by serum proteins but does not affect cell viability for 24 h, as previously reported [20]. Control cells were subjected to the

same treatments except for NP incubation.

2.8. Analysis of cellular uptake of silver and gold NPs

A549 ($1x10^6$) and HBEC3-KT ($0.7 x10^6$) cells were seeded in 60 × 15 mm culture dishes and, after 24 h, were incubated for 24 h with chemically and biogenically synthesized Ag NPs (5 μg/mL) and Au NPs (20 μg/mL). At the end of incubation time cells were fixed in 2.5 % glutaraldehyde in 0.1 M sodium cacodylate buffer as previously reported [21]. Then, samples were post-fixed with a mixture of 1 % osmium tetroxide and 1 % potassium ferrocyanide in 0.1 M sodium cacodylate buffer for 1 h at 4 °C, dehydrated in ethanol from 25 % to 100 % (thrice) for 10 min each step, and finally included in epoxy resin. The samples were sectioned with an Ultrotome V ultramicrotome (LKB instruments, Victoria, TX, USA). Thin sections (80−100 nm) were counterstained with uranyl acetate and lead citrate and then observed at TEM. Images were captured with a Veleta (Olympus Soft Imaging System) digital camera.

2.9. Assessment of cell viability

A549 and HBEC3-KT cells were seeded in triplicate in 96-well plates ($5 x 10^3$ cells/well) in a complete culture medium. After 24 h, cells were incubated for 24 h with increasing concentrations of chemically and biogenically synthesized Ag NPs (0, 2, 5, 10, 15 μg/mL) and Au NPs (0, 10, 20, 40, 60, 80 μg/mL), and then assayed for cell viability by the CellTiter 96® Aqueous One Solution Cell Proliferation Assay (Promega, Madison, WI, USA) as previously reported [20–23]. Briefly, the culture medium was removed, and the cells were incubated for 45 min in the dark with 20 μL of the MTS ((3-(4,5-dimethylthiazol-2-yl)-5-(3-carboxymethoxyphenyl)-2-(4-sulfophenyl)-2H-tetrazolium salt) reagent diluted in 100 μL of serum free medium. The absorbance of the formazan product was measured at 490 nm with a microplate reader (Spectramax 190, Molecular Device, San Jose, CA, USA). Cell viability was determined by comparing the absorbance values of NP-treated cells *vs.* untreated control cells that were considered 100 %.

2.10. Colony forming assay

A549 ($0.35x10^6$) and HBEC3-KT ($0.2x10^6$) cells were plated in 35 × 10 mm culture dishes and allowed to attach for 24 h, then, chemical and biogenic Ag and Au NPs were diluted to appropriate concentrations and applied to the cells. At the end of incubation, cells were detached, counted, and seeded in triplicate in dishes of 60 × 15 mm, each containing 300 cells in 5 mL of complete medium, after performing two dilutions of 1:10 each. The seeded cells were allowed to grow in the incubator for 7 days. Subsequently, the colonies were coloured with crystal violet in 100 % methanol (Sigma-Aldrich, St. Louis, MO, USA), and colonies of ≥50 cells were counted to determine the cloning efficiency (CE) as the proportion of cells that formed colonies to the total number of cells plated, expressed in percentage [20,24]. The following concentrations of NPs were used to assess the clonal forming ability of NP-treated cells: 0, 2, 5 and 10 μg/mL for Ag NPs and 0, 40 and 80 μg/mL for Au NPs.

2.11. Live/dead assay

The viability of A549 and HBEC3-KT cells treated with Ag NPs and Au NPs was assessed using the LIVE/DEAD™ Viability/Cytotoxicity Kit (Invitrogen, ThermoFisher Scientific, Eugene OR, USA) [22]. Cells were plated in amount of $2x10^3$ cells/well in a 96-well plate and 24 h later were treated with NPs for 24 h. At the end of incubation time cells were washed twice with phosphate-buffered saline (PBS) and incubated for 45 min at room temperature in the dark with a solution containing the cell permeant calcein acetoxymethyl ester (calcein-AM, 2 μM), nonfluorescent, and cell impermeant ethidium homodimer-1 (EthD-1, 4 μM). This assay differentiates viable cells by detecting intracellular esterase activity: live cells convert the cell-permeant calcein acetoxymethyl ester into fluorescent calcein, emitting green fluorescence. In contrast, dead cells are stained with ethidium homodimer I, which penetrates cells with compromised membranes and binds to nucleic acids, producing a strong red fluorescence indicative of cell death. Fluorescence was measured with the TECAN Spark fluorimeter (Tecan Life Science) using the appropriate excitation and emission filters (ex/em ~495 nm/~515 nm for calcein; ex/em ~495 nm/~635 nm for EthD-1). As a positive control, some wells were incubated with 70 % methanol for 30 min. Additionally, in some wells, no cells were seeded; instead, 100 μL of 1X PBS and 100 μL of the two-colour staining solution were added as blanks. The percentage of live and dead cells was calculated by comparing the fluorescence values of NP-treated vs. untreated cells that were considered as 100 %.

2.12. Apoptosis assays

The induction of apoptosis was assessed by a fluorometric assay to determine the presence of activated Caspase-3 (Caspase-3 Assay Kit, Abcam®). This test is based on the detection of green fluorescence (ex/em ~ 400 nm/505 nm) produced by the cleavage of the DEVD-AFC substrate (7-amino-4-trifluoromethyl coumarin) into AFC by Caspase-3, an effector caspase involved in the apoptotic cascade. HBEC3-KT cells were seeded in a flat-bottom 96-well plate at a concentration of 2000 cells per well in 200 μL of their growth medium and allowed to proliferate for 24 h. The cells were then incubated for 24 h with 5 μg/mL of chemically and biologically synthesized Ag NPs. After incubation, the medium was removed from the wells and transferred to 1.5 mL microtubes, while 30 μL of growth medium was added to the wells containing the cells to prevent them from drying out. The 1.5 mL microtubes were centrifuged at 200 RCF for 10 min, and the supernatant was discarded. Any pelleted material was resuspended in 20 μL of cold lysis buffer and returned to the wells. The plate was incubated on ice for 10 min. Then, 20 μL of 2X Reaction Buffer containing 10 mM DTT was added to each well. Finally, 1.5 μL of the Caspase-3 substrate was added to achieve a final concentration of approximately 40 μM per well. The plate was incubated at 37 °C with 5 % CO_2, protected from light, for 2 h. Fluorescence (ex/em ~ 400 nm/505 nm) was measured using a TECAN Spark fluorimeter (Tecan Life Science). The obtained values were normalized by subtracting the blank values.

Apoptotic cells were identified by their fragmented morphology of their nuclei stained with DAPI (4′,6-diamidino-2-phenylindole). HBEC3-KT cells ($0.4 x 10^6$) were seeded in 60 × 15 mm culture dishes and 24 h later were incubated for 24 h with chemical and biogenic Ag NPs at concentrations of 2 μg/mL, 5 μg/mL, and 10 μg/mL. At the end of incubation time the cells were detached and processed as previously reported [20] and then observed under a LeicaDM4000 fluorescent microscope (Leica Microsystems, Wetzlar, Germany).

2.13. Cytotoxicity assay in 3D-cultured cells

A549 and HBEC3-KT cells were seeded in U-bottom 96-well plates (Nunclon™ Sphera™ 96-Well, ThermoFisher Scientific, Waltham, MA, USA)) at initial concentrations of 500, 1000, and 2000 cells/well in 200 μL of their respective growth media. The surface coating of pre-treated wells prevents protein adsorption and cell adhesion to the well bottom, minimizing cell adhesion and promoting the assembly of 3D structures. Spheroid formation and growth were assessed using an optical microscope at 48 h, 4 days, and 7 days. The LIVE/DEAD™ Viability/Cytotoxicity Kit (Invitrogen, ThermoFisher Scientific, Eugene OR, USA) was used to qualitatively assess the cytotoxicity induced by 24-h incubation with Ag and Au NPs on A549 and HBEC3-KT spheroids. On the seventh day post-seeding, 140 μL of growth medium was removed from each well, and the spheroids were incubated with chemically and biologically synthesized Ag and Au NPs at a

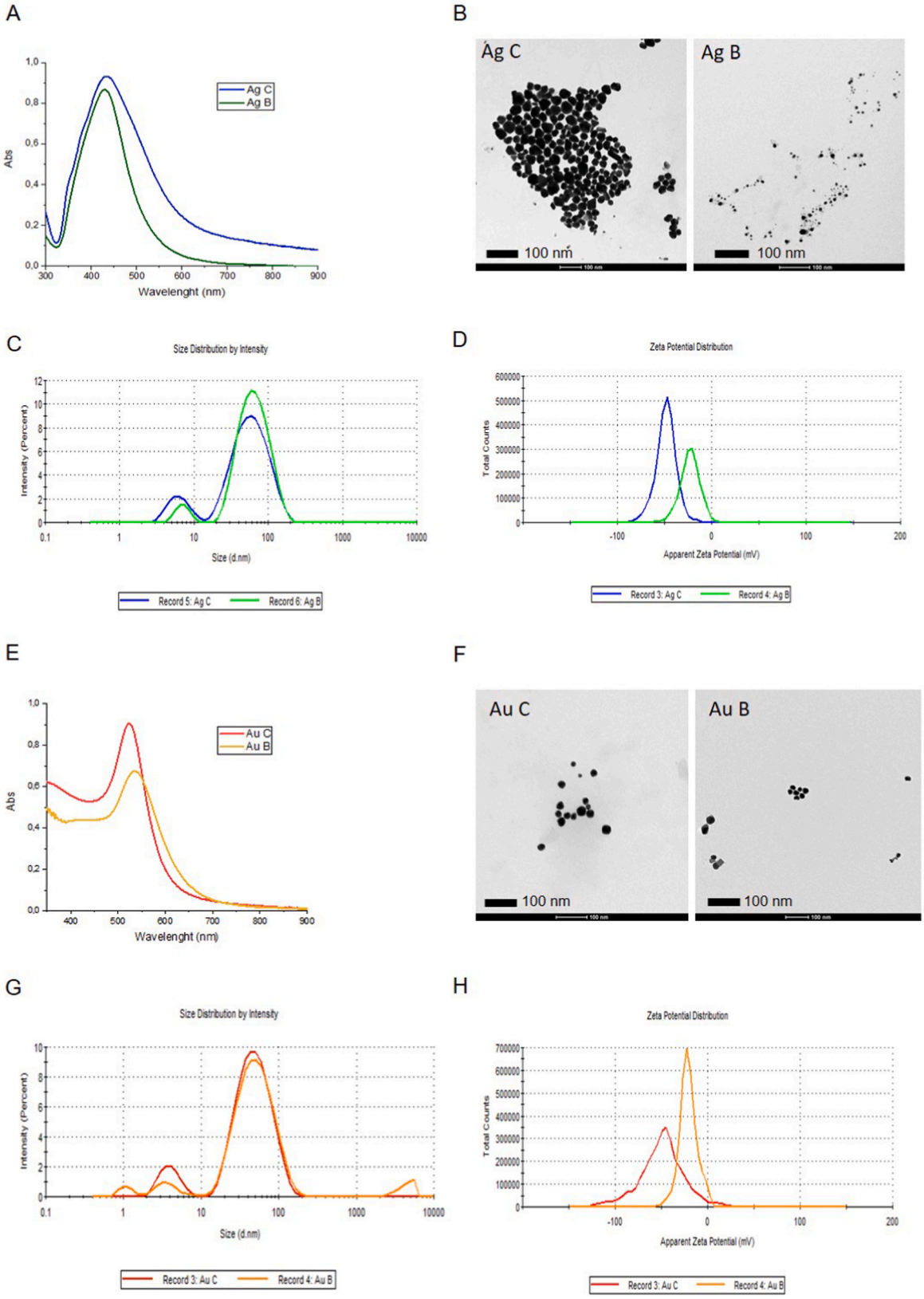

Fig. 1. Characterization of Ag and Au NPs synthesized by chemical or biogenic reduction. A, E) UV–Vis spectra of Ag and Au NPs obtained by chemical (C) and biogenic (B) reduction. B, F) Trasmission electron micrographs (TEM) of NP suspensions. Scale bars are 100 nm. C, G) Hydrodynamic diameter distribution by DLS measurement. D, H) Surface charge of the different nanoparticles evaluated through Zeta potential analysis.

Table 1
DLS characterization of colloidal formulations of NPs.

Sample	D_H (nm)	PDI	Intercept	Zeta Potential (mV)
Ag C	32.39 ± 0.22	0.524 ± 0.008	0.79 ± 0.001	−48.6 ± 1.18
Ag B	48.62 ± 0.26	0.289 ± 0.002	0.90 ± 0.001	−23.1 ± 0.92
Au C	28.88 ± 0.54	0.484 ± 0.005	0.82 ± 0.001	−49.3 ± 0.57
Au B	37.29 ± 0.25	0.439 ± 0.028	0.84 ± 0.001	−20.9 ± 0.40

Values of hydrodynamic diameter (D_H), polydispersity index (PDI) and zeta potential obtained by DLS for the chemical and biogenic silver (Ag C; Ag B) and gold (Au C; Au B) NPs.

concentration of 15 μg/mL regarding the former and of 80 μg/mL for the latter. The desired NP concentrations were achieved by diluting stock solutions in PneumaCult™-Ex Plus Medium (serum-free), supplemented with Hydrocortisone Stock Solution for HBEC3-KT and F12k medium with 3 % FBS for A549, reaching a final volume of 140 μL. After 24 h of incubation, the medium was completely removed, and the LIVE/DEAD assay was performed. The medium was completely removed from the wells, the spheroids were washed with 1X sterile PBS, and then incubated with 150 μL of the dye solution with final concentrations of 2 μM calcein AM and 4 μM EthD-1. The plate was incubated for 40 min at RT in the dark. For HBEC3-KT spheroids, considering their smaller size, the medium removal and PBS washing were performed with a prior centrifugation at 200 RCF for approximately 1 min (Hermle Labor-Technik GmbH-Z 233 MK) thus facilitating complete medium removal without accidental aspiration of the spheroids. The spheroids were then visualized using a LEICA DM14000 inverted fluorescence microscope. As a control for dead cells, some spheroids were incubated with 70 % methanol for 30 min, followed by removal of the methanol, washing with 1X sterile PBS, and incubation with the dye solution.

2.14. Statistical analysis

Data are reported as means ± standard deviation (S.D.) or standard error (S.E.). The differences between groups were evaluated by two-tailed, unpaired Student's *t*-test and differences with a *p*-value <0.05 were considered significant.

3. Results

3.1. Characterization of chemical and biogenic Ag and Au NPs

The freshly obtained aqueous colloidal suspensions of chemically and biogenic Ag and Au NPs (Ag C; Ag B; Au B; Au C) were first characterized by UV–Vis spectra to determine the correct NPs formation (Fig. 1 A). Ag NPs show maximum absorption from 400 to 500 nm while Au NPs are from 500 to 600 nm, as already reported in literature [25]. Transmission electron microscopy (TEM) micrographs further evidenced the presence of spherical monodispersed NPs (Fig. 1 B) with an average size of 30.3 ± 19.8 nm for Ag C NPs, 7.3 ± 5.4 nm for Ag B NPs, 37.8 ± 11 nm for Au C NPs and 18.3 ± 4.9 nm for Au B NPs. Dynamic Light Scattering (DLS) analysis was performed to determine the hydrodynamic diameter of the NPs [26,27] (Fig. 1C). As expected, the hydrodynamic diameters obtained by DLS (Table 1) were higher than the core sizes measured by TEM, due to the contribution of the solvation layer and possible surface-bound biomolecules or stabilizing agents. In addition, DLS generally provides a volume-weighted average, which may emphasize the contribution of larger aggregates if present, whereas TEM offers direct visualization of the dry nanoparticle core, often resulting in smaller and more defined size distributions [28]. In addition to size measurements, Zeta potential analysis was conducted to evaluate

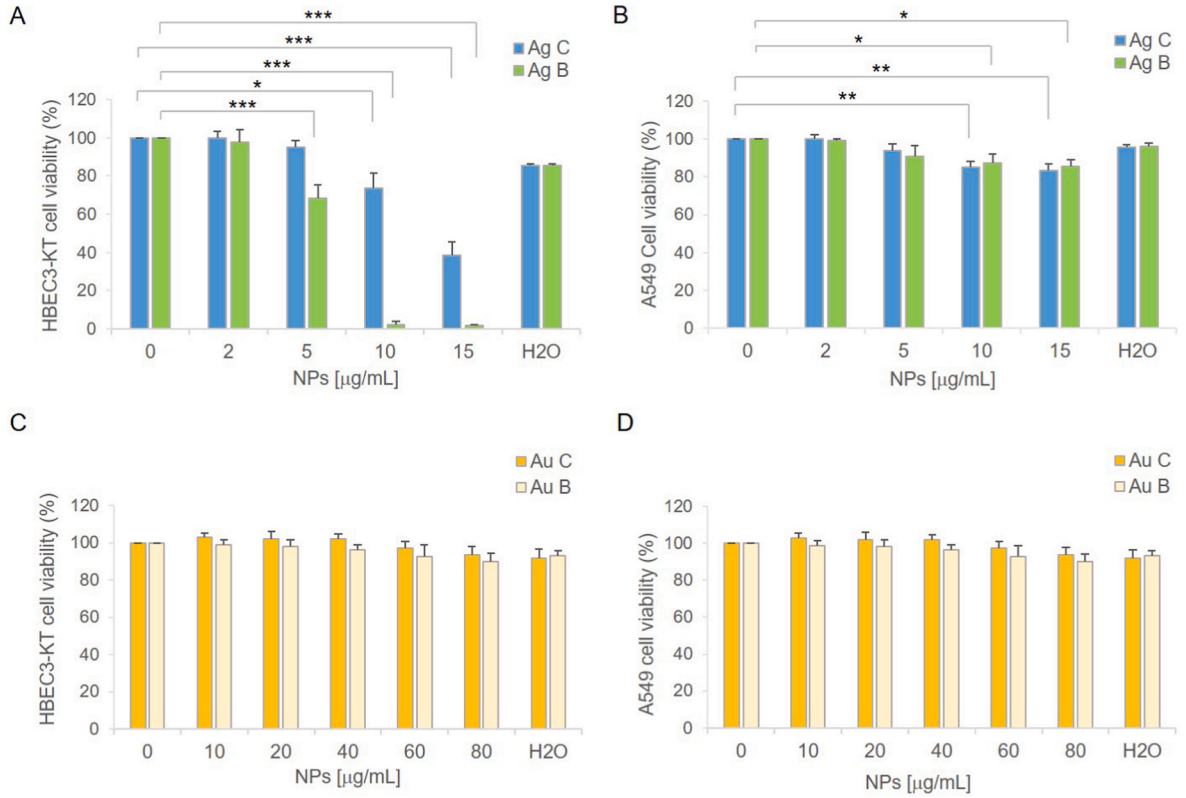

Fig. 2. Cell viability in lung cells incubated with chemical and biogenic Ag and Au NPs. Cell viability was assessed by MTS assay in HBEC3-KT and A549 cells incubated for 24 h with Ag NPs (0–15 μg/mL) and Au NPs (0–80 μg/mL) synthesized by chemical (Ag C; Au C) and biogenic methods (Ag B; Au B). Cells treated with water (H_2O) contained the same volume of water as the highest tested dose and served as a control to assess the effects attributable solely to the water used to suspend the NPs. Data are presented as mean ± S.E. from 3 ≤ n ≤ 5 independent experiments (*$p < 0.05$, **$p < 0.01$, ***$p < 0.001$, Student's *t*-test) carried out on 3–5 different lots of freshly synthesized NPs.

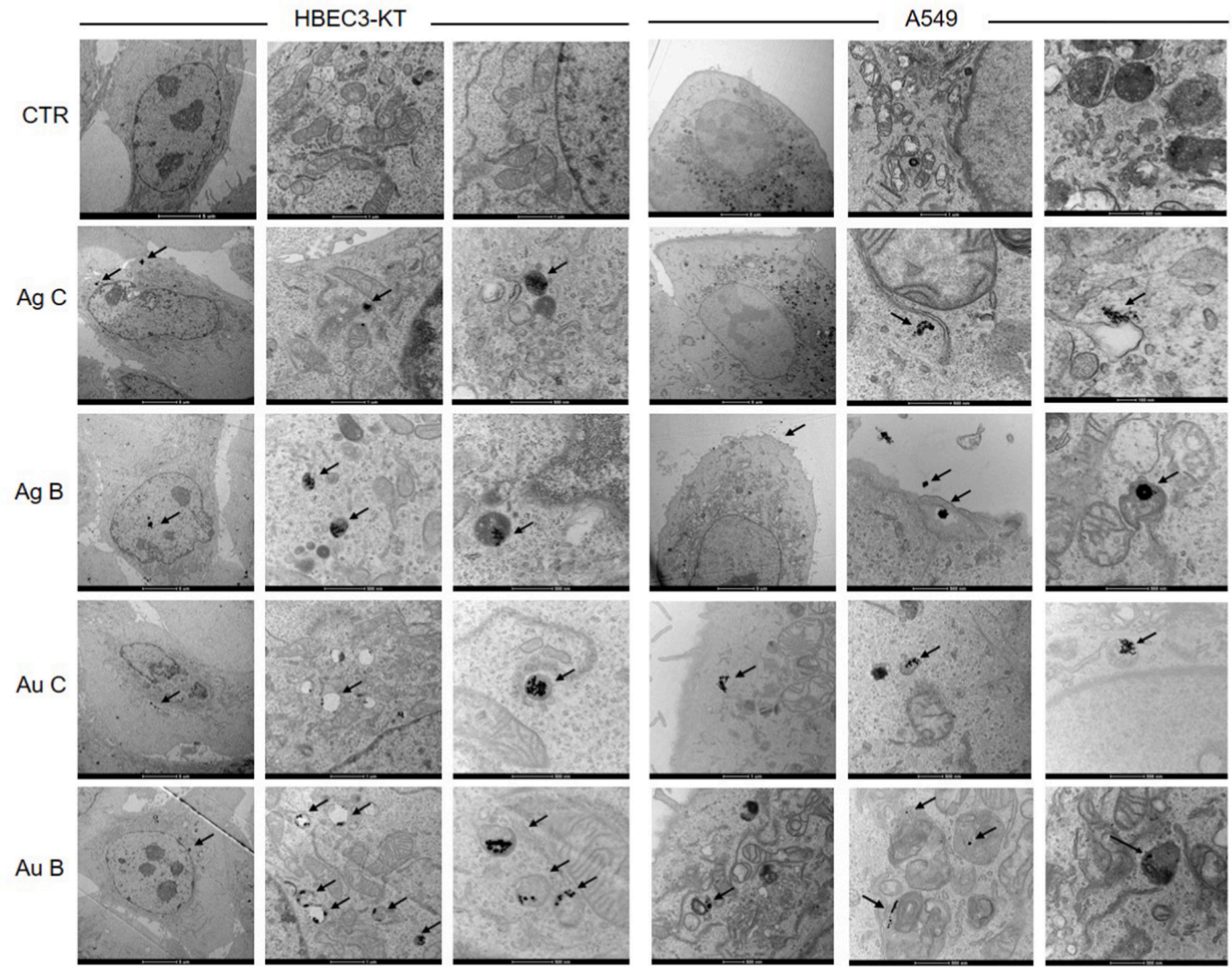

Fig. 3. Cellular uptake of Ag and Au NPs synthesized by chemical and biogenic reduction. TEM images of HBEC3-KT and A549 cells incubated for 24 h with Ag NPs (5 μg/mL) or Au NPs (20 μg/mL) obtained by chemical (C) and biogenic (B) synthesis. The intracellular localization of NPs is indicated by arrows pointing black electron-dense spots.

the surface charge of the NPs. The results showed a highly negative Zeta potential (Ag C: 48.6 mV; Au C: 49.3 mV; Ag B: 23.1 mV; Au B: 20.9 mV; Fig. 1D–H, Table 1), which indicates moderate stability in suspension due to electrostatic repulsion [29]. These characterization results confirmed that the colloidal suspensions of NPs were suitably sized and stable for further cytotoxicity testing.

3.2. Viability of lung cells exposed to chemically and biogenically synthesized NPs

We assessed the impact of chemically and biogenically synthesized Ag and Au NPs on the viability of normal immortalized bronchial cells (HBEC3-KT) and lung adenocarcinoma cells (A549). Cells were cultured in monolayers and exposed to increasing concentrations of NPs colloidal suspensions for 24 h. Following this exposure period, cell viability was assessed by MTS assay. Fig. 2 A shows that Ag NPs at 2 μg/mL did not exhibit toxicity in either cell line, regardless of the synthesis method, however, higher concentrations of NPs affected cell viability differently between the two cell lines. At a concentration of 5 μg/mL, biogenic but not chemical Ag NPs, significantly decreased cell viability of HBEC3-KT cells to 68 % ($p < 0.01$). As the concentration increased, the viability of HBEC3-KT cells was completely compromised by Ag B NPs, whereas Ag C NPs led to a more moderate, but significant, decrease in viability to 74 % ($p < 0.05$) at 10 μg/mL and to 38 % ($p < 0.01$) at 15 μg/mL. The effects of Ag NPs were generally less toxic to A549 cancer cells, with more than 80 % of the cells remaining viable up to 15 μg/mL for both NP suspensions (Fig. 2 B).

Au NP formulations showed minimal cytotoxicity in both cell lines, with cell viability remaining at approximately 95 % with either chemical or biogenic NPs, even at the highest concentration tested (Fig. 2C and D).

3.3. Intracellular uptake of chemical and biogenic Ag and Au NPs

To assess whether the observed cytotoxicity was a result of nanoparticle internalization, we examined the intracellular uptake of Ag and Au NPs in HBEC3-KT and A549 cells after 24 h of incubation. TEM analysis provided clear evidence that both chemical and biogenic Ag and Au NPs were effectively internalized by both cell types in membrane-bound vesicles (Fig. 3). This finding suggests that the cytotoxic effects observed in our previous experiments are likely due to the presence of NPs within the cells, rather than interactions limited to the cell surface.

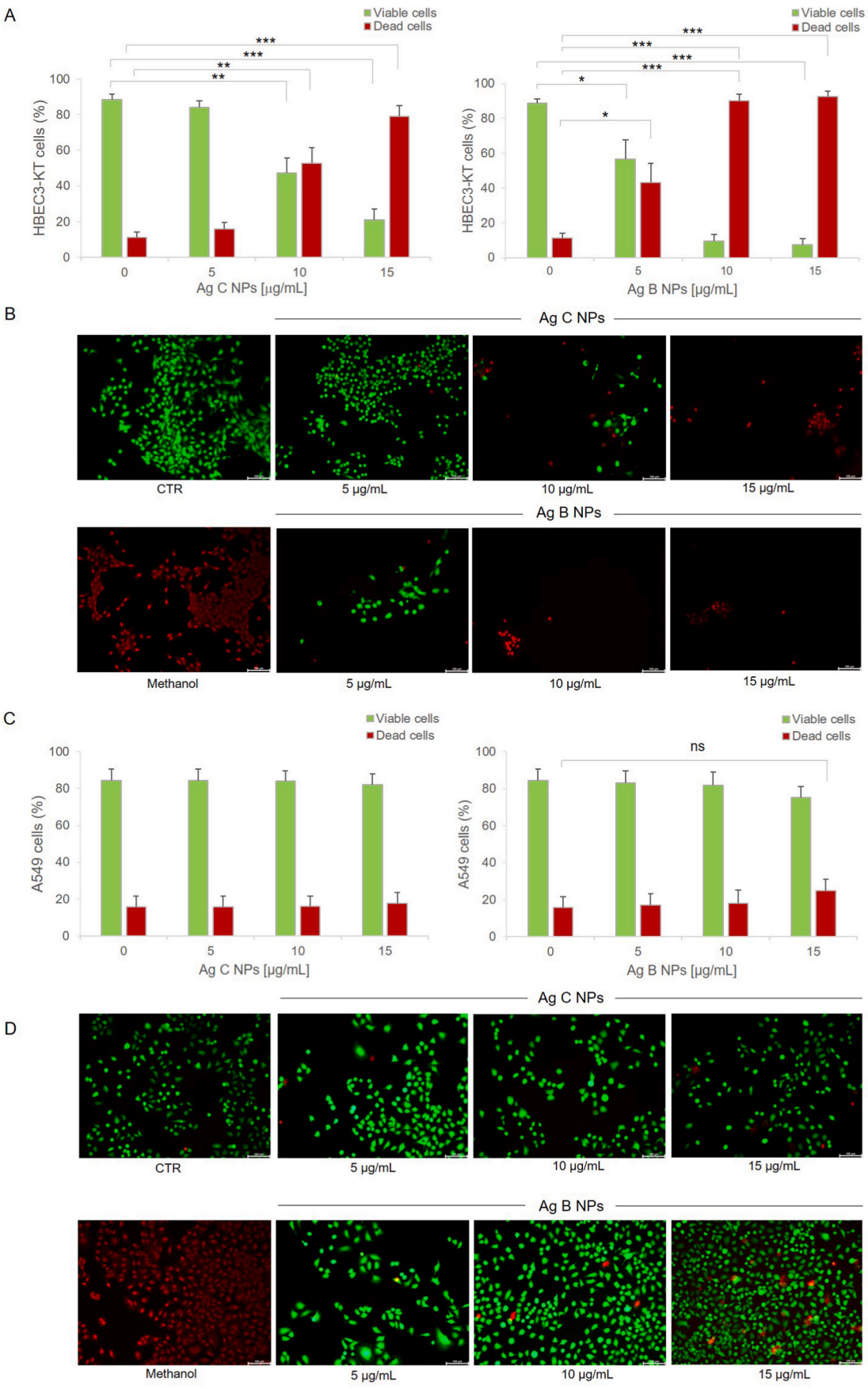

(caption on next page)

Fig. 4. Cytotoxicity of Ag NPs synthesized by chemical and biogenic reduction. Live/Dead® viability/cytotoxicity assay in HBEC3-KT and A549 cells after 24 h of incubation with Ag NPs synthesized via chemical reduction (Ag C) or biogenic reduction (Ag B). The fraction of live and dead HBEC3-KT cells (A) and A549 cells (C) has been determined by fluorimetric analysis. Data are presented as means ± S.D. from three independent experiments performed in 96-microplate wells and analysed by a fluorescence microplate reader (*$p < 0.05$, **$p < 0.01$, ***$p < 0.001$, Student's *t*-test). Representative fluorescence microscopy images of Ag NPs-exposed HBEC3-KT cells (B) and A549 cells (D) stained with calcein AM (green, live cells) and ethidium homodimer-1 (red, dead cells). Cells treated with 70 % methanol for 30 min represent the positive control for death induction. Scale bars: 100 μm. (For interpretation of the references to colour in this figure legend, the reader is referred to the Web version of this article.)

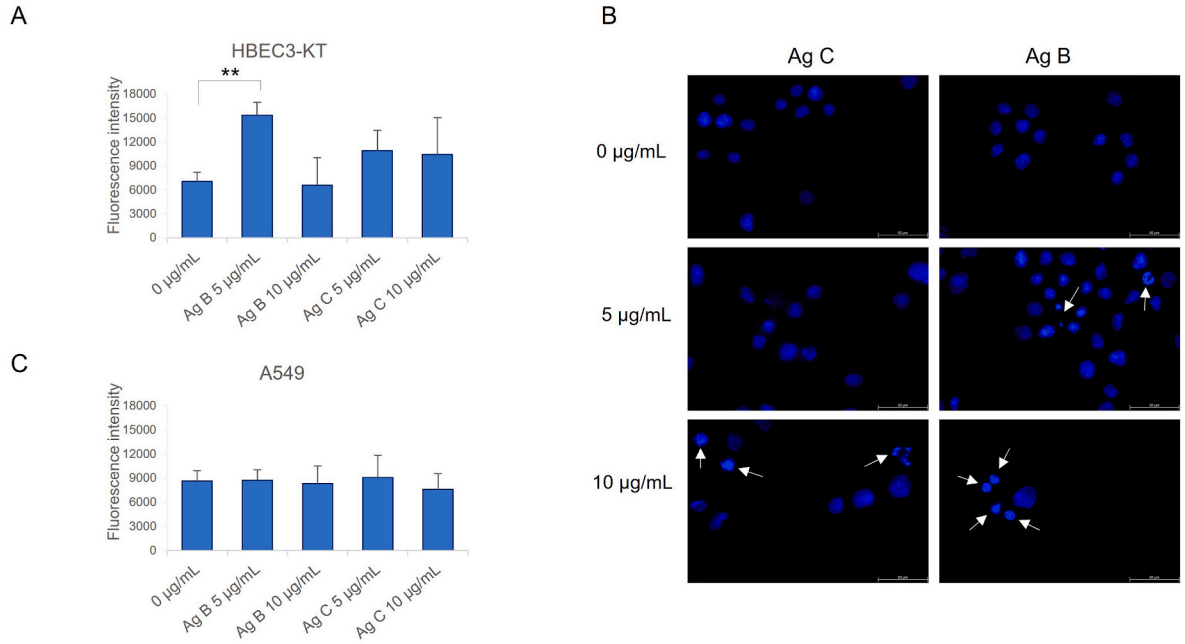

Fig. 5. Induction of apoptosis in HBEC3-KT cells exposed to chemical and biogenic Ag NPs. A) Activation of caspase-3 was measured by fluorimetric analyses 24 h after incubation with chemical (Ag C) and biogenic (Ag B) NPs at concentrations of 5 and 10 μg/mL and in untreated controls (0 μg/mL). The fluorescence intensity data are presented as fold-increase of NP-treated over relative untreated control cells (mean ± S.D. from three independent experiments, **$p < 0.01$, Student's *t*-test). B) Representative images of nuclear DAPI staining with apoptotic cells indicated by white arrows.

3.4. Cytotoxicity of Ag and Au NPs synthesized by chemical and biogenic reduction

We next evaluated the cytotoxicity of Ag and Au NPs in HBEC3-KT and A549 cell lines using the Live/dead assay which revealed distinct patterns of toxicity between the two cell types and NP formulations. Cells were exposed for 24 h to NPs 5, 10, and 15 μg/mL, but not to 2 μg/mL since this concentration did not affect cell viability with MTS assay. In normal HBEC3-KT cells, Ag B NPs 5 μg/mL significantly reduced cell viability to 57 % ($p < 0.05$), while at the same concentration Ag C NPs were no cytotoxic (Fig. 4A and B). At 10 μg/mL, both formulations decreased significantly cell viability, with Ag B NPs causing a more severe reduction (10 % viable and 90 % dead cells, $p < 0.001$) compared to Ag C NPs (47 % viable and 53 % dead cells, $p < 0.01$). At 15 μg/mL, cell death reached 92 % and 79 %, respectively for Ag B and Ag C NPs ($p < 0.001$). In A549 cancer cells both chemical and biogenic Ag NPs did not induce cell death, as the fraction of dead cells was 16–18 % across all concentrations like untreated control cells (Fig. 4C and D). Only Ag B NPs at 15 μg/mL induced the death in 24 % of cells, but this increase was not significant. To investigate if cell death in HBEC3-KT cells occurred by apoptosis, we assessed caspase-3 activation after 24-h exposure to 5 and 10 μg/mL of Ag NPs. At 5 μg/mL, both NP types increased caspase-3 activation, with biogenic NPs showing a significant increase ($p < 0.01$). At 10 μg/mL, caspase-3 remained activated in cells exposed to chemical NPs but decreased in cells treated with biogenic NPs, consistent with the high level of cell death (90 %) observed in the live/dead assay and the presence of numerous apoptotic bodies (Fig. 5 B). Consistent with the low level of cell death observed in the live/dead assay, caspase-3 activation was not detected in A549 cells exposed to Ag NPs at concentrations of 5 and 10 μg/mL for 24 h (Fig. 5C). Regarding Au NPs, both chemical and biogenic formulations showed little toxicity in both cell lines, being live cells 80–90 % after 24-h incubation (Fig. 6).

3.5. Late effects of chemical and biogenic Ag and Au NPs on cell proliferation ability

We further investigated the potential of different NP formulations to cause perturbations at the single-cell level by measuring clonogenic survival in cells treated for 24 h with Ag NPs (2, 5, 10 μg/mL) or with Au NPs (40 and 80 μg/mL). At 2 μg/mL, both chemical and biogenic Ag NPs had no effect on clonogenic survival in HBEC3-KT and A549 cells (Fig. 7A and B). At 5 μg/mL, chemical Ag NPs maintained high clonogenic survival (96 % in HBEC3-KT, 99 % in A549), while biogenic Ag NPs significantly reduced survival to 75 % in HBEC3-KT ($p < 0.05$) and 64 % in A549 ($p < 0.001$). At 10 μg/mL, chemical Ag NPs further reduced survival to 77 % in HBEC3-KT ($p < 0.05$) and 64 % in A549 ($p < 0.001$). Biogenic Ag NPs at this concentration completely prevented HBEC3-KT cell survival since no viable HBEC3-KT cells were recovered after the treatment, while 63 % of A549 cells survived ($p < 0.01$). These results demonstrate that Ag NPs, particularly the biogenic ones, can significantly impact single-cell survival at higher concentrations, in both cell lines. In contrast, Au NPs exhibited minimal effects on clonogenic survival, even at high concentrations, further supporting their lower toxicity profile. Au NPs at 40 μg/mL, neither chemical nor biogenic, affected clonal forming ability in either cell line. At 80 μg/mL, chemical Au NPs maintained approximately 90 % clonogenic survival in both cell

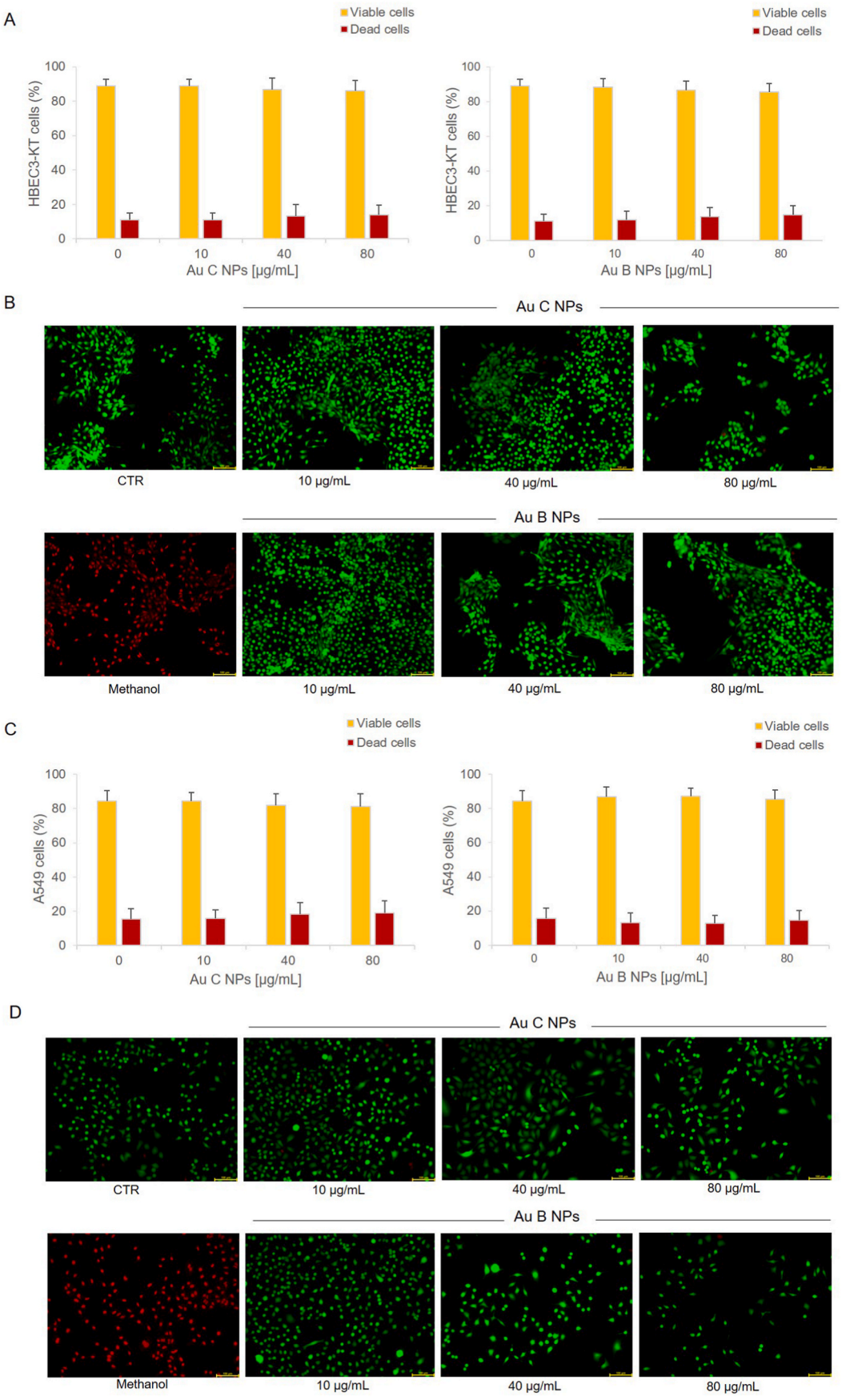

(caption on next page)

Fig. 6. Cytotoxicity of Au NPs synthesized by chemical and biogenic reduction. Live/Dead® viability/cytotoxicity assay in HBEC3-KT and A549 cells after 24 h of incubation with Au NPs synthesized via chemical reduction (Au C) and biogenic reduction (Au B). The fraction of live and dead HBEC3-KT cells (A) and A549 cells (C) has been determined by fluorimetric analysis. Data are presented as means ± S.D. from three independent experiments performed in 96-microplate wells and analysed by a fluorescence microplate reader (*$p < 0.05$, **$p < 0.01$, ***$p < 0.001$, Student's *t*-test). Representative fluorescence microscopy images of HBEC3-KT cells (B) and A549 cells (D) stained with calcein AM (green, live cells) and ethidium homodimer-1 (red, dead cells). Cells treated with 70 % methanol for 30 min represent the positive control for death induction. Scale bars: 100 μm. (For interpretation of the references to colour in this figure legend, the reader is referred to the Web version of this article.)

lines, whereas biogenic Au NPs slightly reduced survival to 76 % in HBEC3-KT and 81 % in A549 cells ($p < 0.05$, Fig. 7C and D). As shown in Fig. 8, the comparison of cell survival derived from the different assays evidence that short-term enzymatic assays are less sensitive compared to the long-term assay in estimating the toxic effects of NPs.

3.6. Cytotoxicity of chemical and biogenic Ag and Au NPs towards cellular spheroids

We tested the effects of chemical and biogenic NPs on seven-day-old spheroids of HBEC3-KT and A549 cells incubated for 24 h with the highest concentrations of Ag and Au NPs (respectively 15 μg/mL and 80 μg/mL). At the end of NPs incubation, spheroids were subjected to the Live/dead assay and observed under a fluorescence microscope. Most cells were viable across all conditions, as visible by the green fluorescence in individual spheroids (Fig. 9). Few dead cells (in red) were observed at the periphery of HBEC3-KT spheroids treated with Ag NPs of both formulations, and with Au B NPs. Notably, the red fluorescence is visible in ungrouped cells, being HBEC3-KT spheroids small, multiple and easily fragmentable. A549 spheroids showed predominantly viable cells after all incubations, except for few dead cells detected at the periphery of spheroids incubated with Ag B NPs.

4. Discussion

The shift towards biogenic synthesis of metallic NPs necessitates a thorough understanding of their biocompatibility and cytotoxicity [30]. The characterization of chemically and biogenically synthesized Ag and Au NPs confirmed their successful synthesis and stability, enabling reliable biological assessments. UV–Vis spectroscopy outlined the expected surface plasmon resonance (SPR) peaks, confirming the formation of Ag and Au NPs, with slightly broader absorption bands for Ag NPs, indicating potential shape variations or aggregation [31–33]. TEM analysis demonstrated however that all NPs were spherical and not aggregated, and that biogenic NPs were smaller than their chemically synthesized counterparts (Fig. 1B–F). Nevertheless, DLS measurements indicated higher hydrodynamic diameters, indicating that the different coating influences the particle surface in solution [34]. Zeta potential analysis showed a higher negative charge for chemical NPs (approximately −50 mV) respect to biogenic NPs (about −20 mV). This negative charge generates electrostatic repulsion that counteracts aggregation and improves NP stability, but as known it may also influence their cellular uptake [35–37], although a hydrodynamic size range between 10 and 60 nm is the most favorable for cellular uptake regardless of zeta potential and NP composition [38].In evaluating the impact of Ag and Au NPs on lung cell viability, Ag NPs, either chemically or biogenically synthesized, resulted more toxic than Au NPs, aligning with the silver's toxic properties [5,30]. Notably, Ag NPs induced more toxicity in normal cells (HBEC3-KT) than in cancer cells (A549), and for normal cells, biogenic Ag NPs resulted more toxic than chemical ones. Starting at 5 μg/mL, biogenic Ag NPs reduced cell viability to 68 %, while chemical Ag NPs showed no effect at this concentration (Fig. 2 A). At higher concentrations, the viability of HBEC3-KT cells was drastically reduced, falling below 10 %, whereas that of cells incubated with chemical Ag NPs progressively declined, reaching 74 % and 38 % with respectively 10 and 15 μg/mL of chemical Ag NPs. The enhanced cytotoxicity of biogenic Ag NPs is likely due to their smaller size, which can lead to increased cellular uptake and more pronounced detrimental effects. In contrast, chemically synthesized Ag NPs resulted less toxic, potentially due to their larger size and stabilizing citrate coating, which may reduce cellular interactions [35]. Au NPs, regardless of synthesis method, exhibited minimal cytotoxicity for both HBEC3-KT and A549 cells, even at the highest concentrations tested (Fig. 2C and D). The intracellular uptake analysis confirmed that both chemical and biogenic colloidal suspensions of Ag and Au NPs were effectively internalized by HBEC3-KT and A549 cells (Fig. 3). This suggests that the observed cytotoxicity of Ag NPs, was mainly driven by intracellular interaction rather than cell surface interactions. Moreover, the minimal toxicity observed from Au NPs correlated with their verified cellular uptake. Live/dead and apoptosis experiments provided further mechanistic insights into Ag NP-induced cytotoxicity. Normal HBEC3-KT cells showed higher levels of cell death when incubated with Ag NPs, especially those biogenic (Fig. 4). The fraction of dead cells caused by Ag B and Ag C was respectively 43 % and 16 % (at 5 μg/mL), 90 % and 53 % (at 10 μg/mL), 92 % and 79 % (at 15 μg/mL). In contrast, cancer A549 cells treated with both formulations of Ag NPs showed a proportion of dead cells comparable to that of control untreated cells (16–18 %), except for a little increase, not significant, at the highest concentration of Ag B NPs. Further analysis indicated that cell death of HBEC3-KT cells occurred by an apoptotic mechanism as evidenced by the activation of caspase-3 activation, whose increase was significant for Ag B NPs (Fig. 5). Conversely to Ag NPs, Au NPs did not induce cell death in both HBEC3-KT and A549 cells (Fig. 6), confirming their biocompatibility [39]. The different level of Ag NPs cytotoxicity observed between the normal and cancer cells came evident from the results of MTS and live/dead assays. As known these assays determine cell viability based on biochemical and physical characteristics of cells, such as enzymatic activities and plasma membrane integrity that may still occur in cell-cycle arrested cells or early apoptotic cells, and that can underestimate the effects of NP treatments. To have a valuable measure of cytotoxicity we investigated the proliferation ability of cells by performing the clonogenic assay which is particularly sensitive since it directly measures the ability of individual NP-treated cells to form colonies of daughter cells [40,41], providing a reliable assessment of their proliferative potential over a 7–10 days period post-treatment. Such assay revealed a significant reduction in the proliferation capacity of A549 cells incubated with Ag NPs that was not evidenced by the short-term MTS and live/dead assays. Specifically, when incubated with biogenic Ag NPs 5 μg/mL, A549 cells significantly decreased their clonogenic survival to 64 % in contrast to a cell survival of 95–100 %, measured respectively with the MTS assay and the Live/Dead assay (Fig. 8). Similarly, the clonogenic survival of A549 cells incubated with Ag NPs 10 μg/mL, either chemical or biogenic, was 64 % when assessed by clonogenic assay, and above 80 % when assessed by short-term assays. Conversely, the data of clonogenic survival of HBEC3-KT cells were in accordance with those determined by short-term assays, with the only exception at 10 μg/mL for the Live/dead assay. These results highlight the importance of the testing strategy and cell type in assessing the toxicity of NPs, as previously reported [20]. The higher cytotoxicity of biogenic Ag NPs towards normal HBEC3-KT cells compared to cancer A549 cells, as demonstrated by both short- and long-term assays, is related to physiological differences between the malignant and non-malignant states. These differences include metabolic activity, proliferation rate, oxidative stress response, gene expression alterations, that ultimately can influence cell death [42–45] Due to their heightened metabolic activity, cancer cells tend to have higher ROS levels than

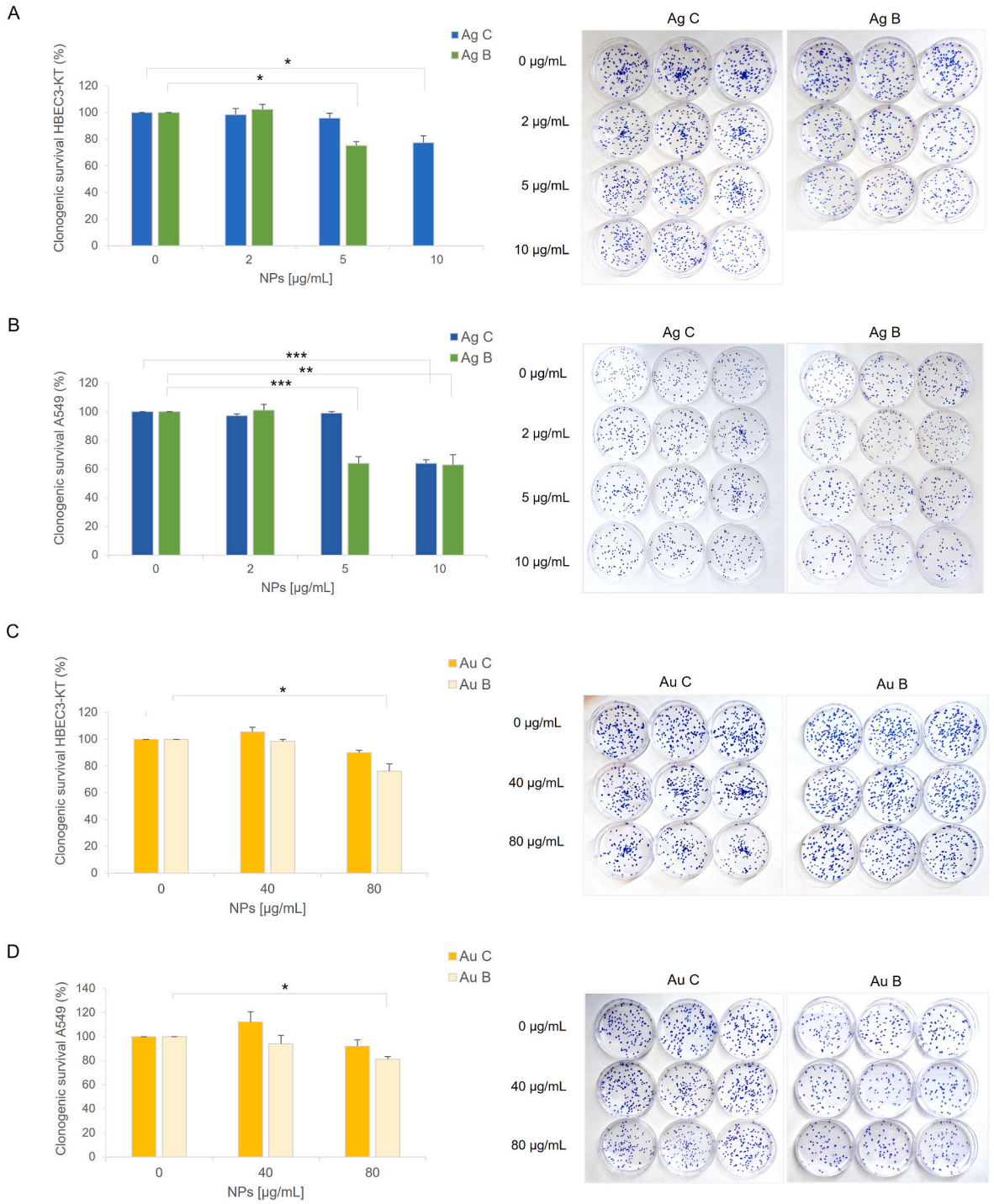

Fig. 7. Colony forming ability of HBEC3-KT and A549 cells incubated with chemical and biogenic NPs. Cells were incubated for 24 h with chemical and biogenic Ag NPs (0-2-5-10 μg/mL), or Au NPs (0-40-80 μg/mL) and the values of cloning efficiency (CE) were used to calculate clonogenic cell survival, expressed as the percentage of the CE of NP-treated cells over that of untreated control cells (100 %). Data report means ± S.E. from independent experiments ($3 \leq n \leq 5$), each conducted in triplicate (*$p < 0.05$, **$p < 0.01$, ***$p < 0.001$, Student's *t*-test). HBEC3-KT cells incubated with Ag NPs (A); A549 cells incubated with Ag NPs (B); HBEC3-KT cells incubated with Au NPs (C); A549 cells incubated with Au NPs (D). Representative images of clones derived from cells incubated for 24 h with Ag and Au NPs are shown. Note: At 10 μg/mL of biogenic Ag NPs, no viable HBEC3-KT cells were recovered, preventing the performance of the clonogenic assay.

normal cells, therefore cell death induction in cancer cells requires the exceed of their ROS threshold by specifically targeting antioxidant proteins [46]. A549 cells proved to be less susceptible to oxidative stress than normal cells [20,42] which may contribute to their resistance against cytotoxicity induced by NPs of various origins, and high doses of ionizing radiation [24,47,48].

Gold NPs, in contrast to silver ones, showed similar results across the different assays, including the clonogenic one which confirmed a cell survival above 75 % with both type of formulations even at the highest tested dose (Fig. 7C and D), supporting the high biocompatibility of Au NPs. These findings agree with previous studies highlighting how NP-induced cytotoxicity is influenced by NP characteristics, cell type, and assay type used to assess cytotoxicity [20,49]. NP size has been identified as a key factor influencing cytotoxicity, with smaller NPs generally

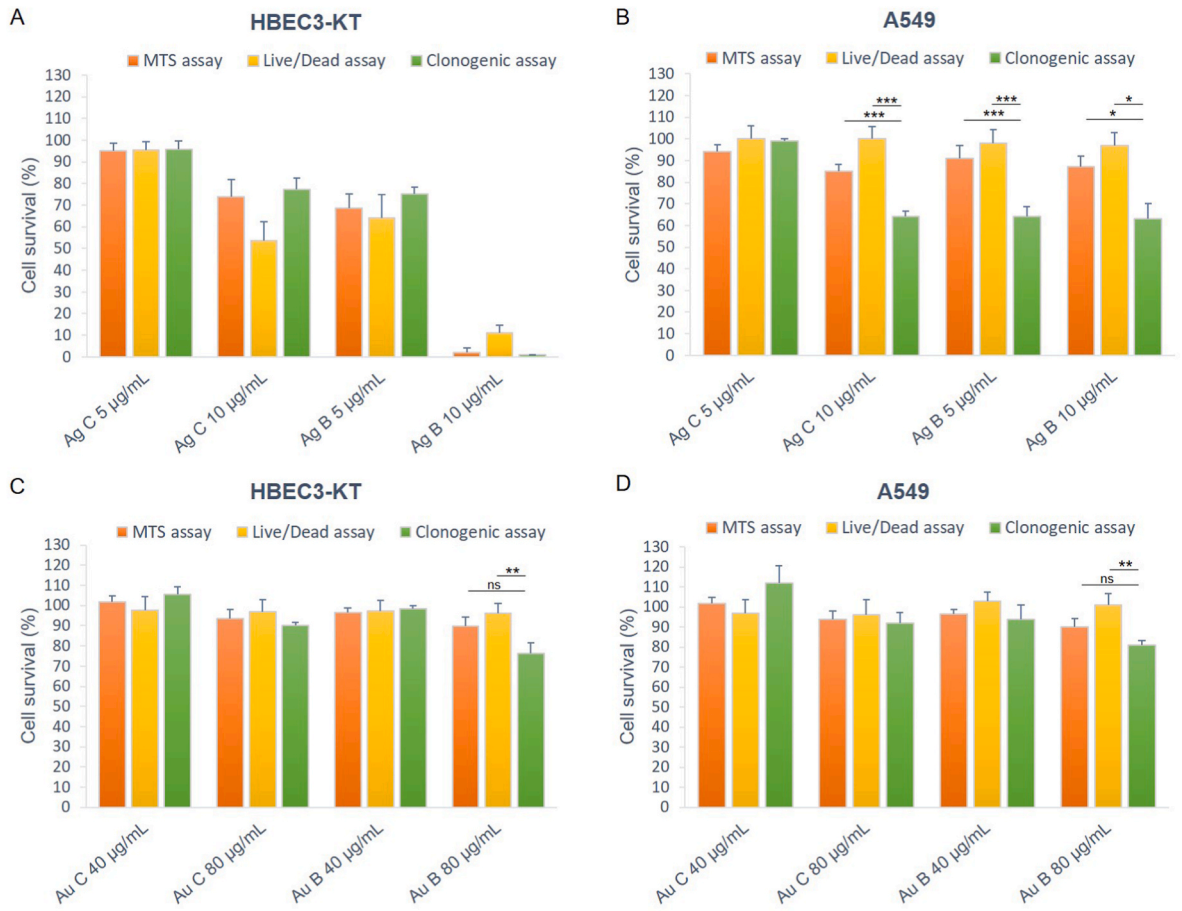

Fig. 8. Cell survival determined by MTS, Live/dead and clonogenic assays in HBEC3-KT and A549 cells incubated with chemical and biogenic Ag and Au NPs. The data, derived from assays carried out on 3–5 different batches of freshly synthesized NPs, are expressed as the proportion of NP-treated vs. untreated control cells expressed in percentage (*$p < 0.05$, **$p < 0.01$, ***$p < 0.001$, Student's *t*-test).

exhibiting higher toxicity compared to larger NPs [50–52]. Ag NPs of approximately 60 nm in diameter induced significant cytotoxicity in A549 cells at 50 µg/mL [53], whereas in the same cells, smaller NPs of 10–15 nm in diameter showed toxic effects at concentrations as low as 10 µg/mL [54]. Our findings support the notion that biogenically synthesized Ag NPs, that have a smaller average size (~7 nm) exhibit greater cytotoxicity than their chemically synthesized counterparts, which have a larger average size (~30 nm). Among the Au NPs only the biogenic ones slightly impacted the clonogenic survival of both cell types at the highest concentration tested (80 µg/mL), denoting their low cytotoxicity. Most studies have evaluated the cytotoxicity of Au NPs against cancer cells, and biosynthesized Au NPs have demonstrated varying levels of toxicity in A549 cells across different studies. Abdallah et al. [55] reported no toxicity within a concentration range of 0–150 µg/mL. However, Uboldi et al. [56] observed slight toxicity at approximately 140 µg/mL. In contrast, Anandan [57] found that biosynthesized Au NPs reduced A549 cell viability by 50 % at 100 µg/mL, with initial signs of toxicity evident as early as 40 µg/mL. These disparate findings highlight the variability in cytotoxic effects of biosynthesized Au NPs, which may be attributed to differences in synthesis methods, particle characteristics (i.e. size, zeta potential, surface chemistry), and/or experimental conditions. Our results align with other reports, where smaller Au NPs (5 nm) exhibited more pronounced toxic effects compared to larger particles (50 nm) at the same concentration in HBEC3-KT [58]. This size-dependent toxicity has also been demonstrated in HeLa cells, where smaller NPs (4.8 nm) reduced cell viability to 50 % at 50 µg/mL, while larger NPs (46.6 nm) resulted in 90 % viability at the same concentration [59]. The difference in toxicity observed between the biogenic and chemically synthesized Au NPs used in this study may be attributed to the smaller size of the biogenic particles compared to the chemically synthesized ones (respectively 18.3 ± 4.9 and 37.8 ± 11 nm).

Finally, the evaluation of NP effects in cellular spheroids confirmed the differential cytotoxicity of Ag and Au NPs observed in monolayer cultures. In general, the high concentration of NPs tested little impacted on cell viability of HBEC3-KT and A549 spheroids (Fig. 9). Low levels of cell death were observed at the periphery of HBEC3-KT and A549 spheroids incubated with biogenic Ag NPs following interactions with the outermost cells than the middle or core ones. Chemically synthesized Ag NPs induced a similar effect in HBEC3-KT spheroids but had a weaker impact on A549 spheroids. The observed differences could be attributed to the normal and cancer status of cells forming the spheroids, with normal cells more susceptible than cancer cells to cell death induction by NPs. Moreover, NPs may have less efficient penetration into the multicellular layers of spheroids than in monolayer cultures, potentially requiring higher concentrations to induce toxicity. Exposure of spheroids to Au NPs revealed no dead cells on the outer layer of either cell line's spheroids, despite the abundance of visible NPs on the cells, further supporting their biocompatibility.

The limitations of the proposed protocol are mainly attributed to the novelty of the proposed biogenic approach which needs to be optimized and standardized in terms of involved experimental parameters to better control size and shape of NPs. Moreover, further studies are necessary to explore the impact of such metallic NPs in in vivo human/animal biological systems with a three-dimensional tissue organization, focusing on cellular uptake, biodistribution, tissue inflammation and

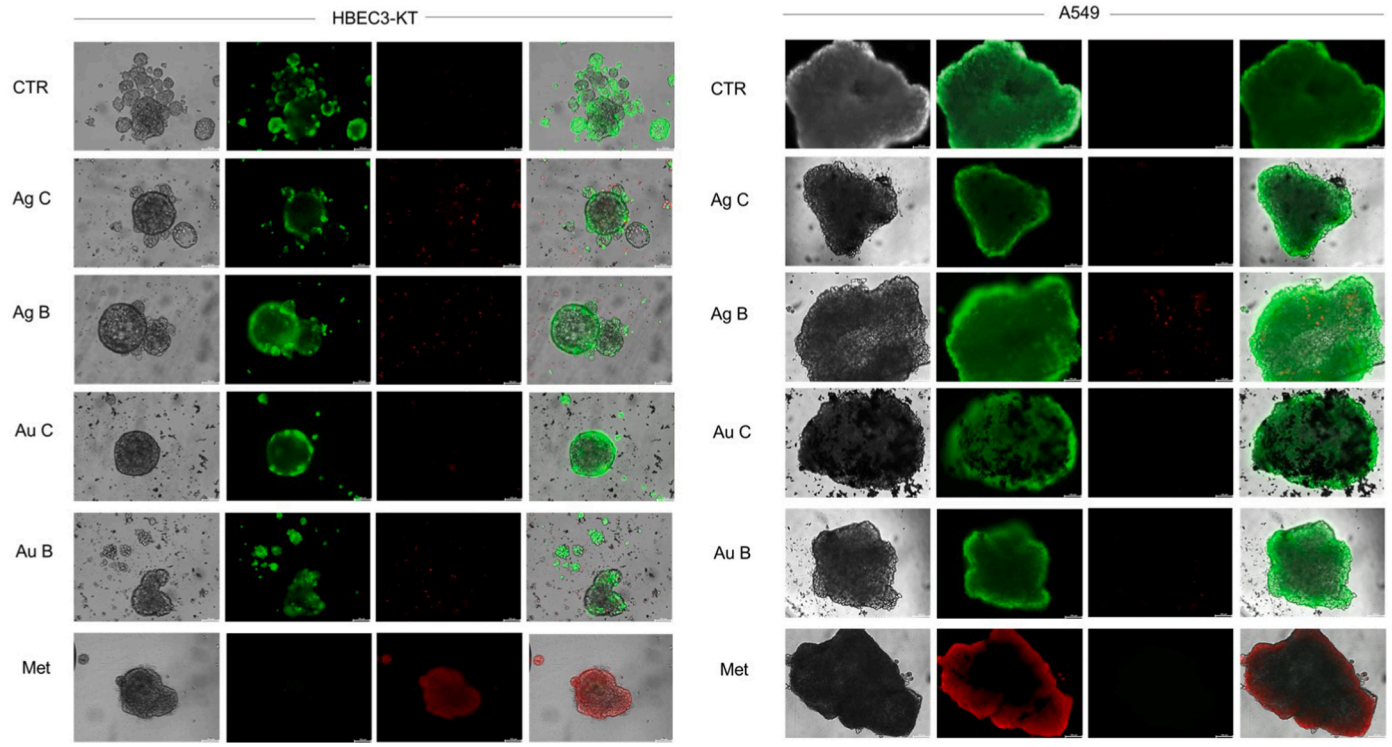

Fig. 9. Live/Dead assay for the determination of cell viability in spheroids of HBEC3-KT and A549 cells exposed to chemical and biogenic NPs. Seven-day-old spheroids were incubated for 24 h with Ag C or Ag B NPs (15 μg/mL) and with Au C or Au B NPs (80 μg/mL). Fluorescence microscopy images of spheroids showing live cells in green, and dead cells in red. Spheroids treated with 70 % methanol (Met) for 30 min represent the positive control for death induction. Scale bar: 100 μm. (For interpretation of the references to colour in this figure legend, the reader is referred to the Web version of this article.)

genotoxicity.

5. Conclusions

This study presents experimental evidence that biogenic Ag NPs exhibit stronger cytotoxic effects than chemically synthesized Ag NPs, suggesting their potential for antimicrobial or anticancer applications. Conversely, the low toxicity of biogenic Au NPs indicates their suitability for biomedical applications requiring high biocompatibility. Notably, our research uncovered a higher sensitivity of normal cells compared to cancer cells towards Ag NP toxicity. This crucial observation emphasises the need for comprehensive and strategic testing protocols in evaluating the safety and therapeutic potential of these NPs across various biomedical fields.

CRediT authorship contribution statement

Martina Leoncini: Methodology, Validation, Writing – review & editing. **Chiara Ortile:** Validation, Methodology, Investigation, Data curation. **Susanna Tinello:** Writing – review & editing, Methodology, Formal analysis. **Silvia Gross:** Writing – review & editing, Supervision, Methodology, Investigation, Data curation, Conceptualization. **Maddalena Mognato:** Writing – review & editing, Writing – original draft, Supervision, Investigation, Funding acquisition, Data curation.

Declaration of generative AI and AI-assisted technologies in the writing process

During the preparation of this work the authors used Lucrez-IA UNIPD tool of the Digital Learning e Multimedia Office (ASIT) of the University of Padova, in order to improve the readability of the manuscript. After using this tool, the authors reviewed and edited the content as needed and take full responsibility for the content of the publication.

Funding

This work was supported by the University of Padova (BIRD-DOR to MM).

Declaration of competing interest

The authors declare that they have no known competing financial interests or personal relationships that could have appeared to influence the work reported in this paper.

Acknowledgments

We thank Dr. Francesco Boldrin and Dr. Federico Caicci (Department of Biology, University of Padova) for TEM analyses. Francesco Rosato (Department of Chemical Sciences, University of Padova) is gratefully acknowledged for his technical support.

Data availability

Data will be made available on request.

References

[1] M.G. Heinemann, C.H. Rosa, G.R. Rosa, D. Dias, Biogenic synthesis of gold and silver nanoparticles used in environmental applications: a review, Trends Environ. Anal. Chem. 30 (2021) e00129, https://doi.org/10.1016/j.teac.2021.e00129.
[2] L. Wei, J. Lu, H. Xu, A. Patel, Z.-S. Chen, G. Chen, Silver nanoparticles: synthesis, properties, and therapeutic applications, Drug Discov. Today 20 (5) (2015) 595–601, https://doi.org/10.1016/j.drudis.2014.11.014.
[3] S. Onitsuka, T. Hamada, H. Okamura, Preparation of antimicrobial gold and silver nanoparticles from tea leaf extracts, Colloids Surf. B Biointerfaces 173 (2019) 242–248, https://doi.org/10.1016/j.colsurfb.2018.09.055.
[4] Y.-C. Yeh, B. Creran, V.M. Rotello, Gold nanoparticles: preparation, properties, and applications in bionanotechnology, Nanoscale 4 (6) (2012) 1871–1880, https://doi.org/10.1039/C1NR11188D.

[5] P. Talarska, M. Boruczkowski, J. Żurawski, Current knowledge of silver and gold nanoparticles in laboratory research—application, toxicity, cellular uptake, Nanomaterials 11 (9) (2021) 2454, https://doi.org/10.3390/nano11092454.

[6] K.N. Thakkar, S.S. Mhatre, R.Y. Parikh, Biological synthesis of metallic nanoparticles, Nanomed. Nanotechnol. Biol. Med. 6 (2) (2010) 257–262, https://doi.org/10.1016/j.nano.2009.07.002.

[7] E. García-Garrido, M. Cordani, Á. Somoza, Modified gold nanoparticles to overcome the chemoresistance to gemcitabine in mutant p53 cancer cells, Pharmaceutics 13 (12) (2021 Dec 3) 2067, https://doi.org/10.3390/pharmaceutics13122067.

[8] M. Ghobadi, S. Salehi, M.T.S. Ardestani, M. Mousavi-Khattat, Z. Shakeran, A. Khosravi, M. Cordani, A. Zarrabi, Amine-functionalized mesoporous silica nanoparticles decorated by silver nanoparticles for delivery of doxorubicin in breast and cervical cancer cells, Eur. J. Pharm. Biopharm. 201 (2024 Aug) 114349, https://doi.org/10.1016/j.ejpb.2024.114349.

[9] L. Fan, W. Wang, Z. Wang, M. Zhao, Gold nanoparticles enhance antibody effect through direct cancer cell cytotoxicity by differential regulation of phagocytosis, Nat. Commun. 12 (1) (2021 Nov 4) 6371, https://doi.org/10.1038/s41467-021-26694-x.

[10] Y.C. Chen, L.C. Chang, Y.L. Liu, M.C. Chang, Y.F. Liu, P.Y. Chang, D. Manoharan, W.J. Wang, J.S. Chen, H.C. Wang, W.T. Chiu, W.P. Li, H.S. Sheu, W.P. Su, C.S. Yeh, Redox disruption using electroactive liposome coated gold nanoparticles for cancer therapy, Nat. Commun. 16 (1) (2025 Apr 5) 3253, https://doi.org/10.1038/s41467-025-58636-2.

[11] Tarannum, N.; Divya; K. Gautam, Y. Facile Green Synthesis and Applications of Silver Nanoparticles: A State-of-the-Art Review. *RSC Adv.* **2019**, *9* (60), 34926–34948. https://doi.org/10.1039/C9RA04164H.

[12] S. Gross, *Unconventional Green Synthesis of Inorganic Nanomaterials*, Royal Society of Chemistry (2024).

[13] M. Wuithschick, A. Birnbaum, S. Witte, M. Sztucki, U. Vainio, N. Pinna, K. Rademann, F. Emmerling, R. Kraehnert, J. Polte, Turkevich in new robes: key questions answered for the most common gold nanoparticle synthesis, ACS Nano 9 (7) (2015) 7052–7071, https://doi.org/10.1021/acsnano.5b01579.

[14] P.C. Lee, D. Meisel, Adsorption and Surface-Enhanced Raman of Dyes on Silver and Gold Sols, J. Phys. Chem. 86 (17) (1982) 3391–3395. https://doi.org/10.1021/j100214a025.

[15] J. Turkevich, P.C. Stevenson, J. Hillier, A Study of the Nucleation and Growth Processes in the Synthesis of Colloidal Gold, Discuss. Faraday Soc. 11 (0) (1951) 55–75. https://doi.org/10.1039/DF9511100055.

[16] S. K. Nune, N. Chanda, R. Shukla, K. Katti, R. R. Kulkarni, S. Thilakavathy, S. Mekapothula, R. Kannan, V. Katti, K. Green, Nanotechnology from tea: phytochemicals in tea as building blocks for production of biocompatible gold nanoparticles, J. Mater. Chem. 19 (19) (2009) 2912–2920, https://doi.org/10.1039/B822015H.

[17] A.F. Ismael, N.M. Ahmed, K.H. Ibrahim, A.A. AL-Kubaisi, Tea plant leaves for green synthesis of metallic nanoparticles, Macromol. Symp. 407 (1) (2023) 2100377, https://doi.org/10.1002/masy.202100377.

[18] P. Schlinkert, E. Casals, M. Boyles, U. Tischler, E. Hornig, N. Tran, J. Zhao, M. Himly, M. Riediker, G.J. Oostingh, V. Puntes, A. Duschl, The oxidative potential of differently charged silver and gold nanoparticles on three human lung epithelial cell types, J. Nanobiotechnol. 13 (1) (2015) 1, https://doi.org/10.1186/s12951-014-0062-4.

[19] L. Oprica, M. Andries, L. Sacarescu, L. Popescu, D. Pricop, D. Creanga, M. Balasoiu, Citrate-silver nanoparticles and their impact on some environmental beneficial fungi, Saudi J. Biol. Sci. 27 (12) (2020) 3365–3375, https://doi.org/10.1016/j.sjbs.2020.09.004.

[20] C. Fede, F. Selvestrel, C. Compagnin, M. Mognato, F. Mancin, E. Reddi, L. Celotti, The toxicity outcome of silica nanoparticles (Ludox®) is influenced by testing techniques and treatment modalities, Anal. Bioanal. Chem. 404 (6) (2012) 1789–1802, https://doi.org/10.1007/s00216-012-6246-6.

[21] A.F. De Fazio, G. Morgese, M. Mognato, C. Piotto, D. Pedron, G. Ischia, V. Causin, J.-G. Rosenboom, E.M. Benetti, S. Gross, Robust and biocompatible functionalization of ZnS nanoparticles by catechol-bearing poly(2-methyl-2-oxazoline)s, Langmuir 34 (38) (2018) 11534–11543, https://doi.org/10.1021/acs.langmuir.8b02287.

[22] Zanin A, Meneghetti G, Menilli L, Tesoriere A, Argenton F, Mognato M. Analysis of Radiation Toxicity in Mammalian Cells Stably Transduced with Mitochondrial *Stat3*. Int J Mol Sci. 2023 May 4;24(9):8232. doi: 10.3390/ijms24098232. Erratum in: Int J Mol Sci. 2024 Mar 26;25(7):3672. doi: 10.3390/ijms25073672. PMID: 37175941; PMCID: PMC10179518.

[23] F. Tajoli, N. Dengo, M. Mognato, P. Dolcet, G. Lucchini, A. Faresin, J.-D. Grunwaldt, X. Huang, D. Badocco, M. Maggini, C. Kübel, A. Speghini, T. Carofiglio, S. Gross, Microfluidic crystallization of surfactant-free doped zinc sulfide nanoparticles for optical bioimaging applications, ACS Appl. Mater. Interfaces 12 (39) (2020) 44074–44087, https://doi.org/10.1021/acsami.0c13150.

[24] C. Piotto, A. Biscontin, C. Millino, M. Mognato, Functional validation of miRNAs targeting genes of DNA double-strand break repair to radiosensitize non-small lung cancer cells, Biochim. Biophys. Acta BBA - Gene Regul. Mech. 1861 (12) (2018) 1102–1118, https://doi.org/10.1016/j.bbagrm.2018.10.010.

[25] F. Frederix, J.-M. Friedt, K.-H. Choi, W. Laureyn, A. Campitelli, D. Mondelaers, G. Maes, G. Borghs, Biosensing based on light absorption of nanoscaled gold and silver particles, Anal. Chem. 75 (24) (2003) 6894–6900, https://doi.org/10.1021/ac0346609.

[26] Z. Bahmanyar, F. Mohammadi, A. Gholami, M. Khoshneviszadeh, Effect of different physical factors on the synthesis of spherical gold nanoparticles towards cost-effective biomedical applications, IET Nanobiotechnol. 17 (1) (2023) 1–12, https://doi.org/10.1049/nbt2.12100.

[27] N.A. Begum, S. Mondal, S. Basu, R.A. Laskar, D. Mandal, Biogenic synthesis of Au and Ag nanoparticles using aqueous solutions of black tea leaf extracts, Colloids Surf. B Biointerfaces 71 (1) (2009) 113–118, https://doi.org/10.1016/j.colsurfb.2009.01.012.

[28] E. Tomaszewska, K. Soliwoda, K. Kadziola, B. Tkacz-Szczesna, G. Celichowski, M. Cichomski, W. Szmaja, J. Grobelny, Detection limits of DLS and UV-vis spectroscopy in characterization of polydisperse nanoparticles colloids, J. Nanomater. 2013 (1) (2013) 313081, https://doi.org/10.1155/2013/313081.

[29] S. Skoglund, J. Hedberg, E. Yunda, A. Godymchuk, E. Blomberg, I. Odnevall Wallinder, Difficulties and flaws in performing accurate determinations of zeta potentials of metal nanoparticles in complex solutions—four case studies, PLoS One 12 (7) (2017) e0181735, https://doi.org/10.1371/journal.pone.0181735.

[30] Gold and Silver Nanoparticles: Synthesis and Applications (Micro and Nano Technologies) (Paperback). McNally Jackson Books. https://www.mcnallyjackson.com/book/9780323994545 (accessed 2025-February-19).

[31] M. Lismont, L. Dreesen, Comparative study of Ag and Au nanoparticles biosensors based on surface plasmon resonance phenomenon, Mater. Sci. Eng. C 32 (6) (2012) 1437–1442, https://doi.org/10.1016/j.msec.2012.04.023.

[32] J.M. Zook, V. Rastogi, R.I. MacCuspie, A.M. Keene, J. Fagan, Measuring agglomerate size distribution and dependence of localized surface plasmon resonance absorbance on gold nanoparticle agglomerate size using analytical ultracentrifugation, ACS Nano 5 (10) (2011) 8070–8079, https://doi.org/10.1021/nn202645b.

[33] O. Kvítek, J. Siegel, V. Hnatowicz, V. Švorčík, Noble metal nanostructures influence of structure and environment on their optical properties, J. Nanomater. 2013 (1) (2013) 743684, https://doi.org/10.1155/2013/743684.

[34] Yu V. Larichev, Application of DLS for metal nanoparticle size determination in supported catalysts, Chem. Pap. 75 (5) (2021) 2059–2066, https://doi.org/10.1007/s11696-020-01454-1.

[35] T.L. Doane, C.-H. Chuang, R.J. Hill, C. Burda, Nanoparticle ζ -potentials, Acc. Chem. Res. 45 (3) (2012) 317–326, https://doi.org/10.1021/ar200113c.

[36] E. Fröhlich, The role of surface charge in cellular uptake and cytotoxicity of medical nanoparticles, Int. J. Nanomed. 7 (2012) 5577–5591, https://doi.org/10.2147/IJN.S36111.

[37] K. Öztürk, M. Kaplan, S. Çalış, Effects of nanoparticle size, shape, and zeta potential on drug delivery, Int. J. Pharm. 666 (2024) 124799, https://doi.org/10.1016/j.ijpharm.2024.124799.

[38] P. Sabourian, G. Yazdani, S.S. Ashraf, M. Frounchi, S. Mashayekhan, S. Kiani, A. Kakkar, Effect of physico-chemical properties of nanoparticles on their intracellular uptake, Int. J. Mol. Sci. 21 (21) (2020) 8019, https://doi.org/10.3390/ijms21218019.

[39] M. Kus-Liśkiewicz, P. Fickers, I. Ben Tahar, Biocompatibility and cytotoxicity of gold nanoparticles: recent advances in methodologies and regulations, Int. J. Mol. Sci. 22 (20) (2021) 10952, https://doi.org/10.3390/ijms222010952.

[40] N. Brix, D. Samaga, C. Belka, H. Zitzelsberger, K. Lauber, Analysis of clonogenic growth in vitro, Nat. Protoc. 16 (11) (2021) 4963–4991, https://doi.org/10.1038/s41596-021-00615-0.

[41] N.A.P. Franken, H.M. Rodermond, J. Stap, J. Haveman, C. van Bree, Clonogenic assay of cells in vitro, Nat. Protoc. 1 (5) (2006) 2315–2319, https://doi.org/10.1038/nprot.2006.339.

[42] L. Zhang, W. Zhou, V.E. Velculescu, S.E. Kern, R.H. Hruban, S.R. Hamilton, B. Vogelstein, K.W. Kinzler, Gene expression profiles in normal and cancer cells, Science 276 (5316) (1997) 1268–1272, https://doi.org/10.1126/science.276.5316.1268.

[43] Z. Bar-Joseph, Z. Siegfried, M. Brandeis, B. Brors, Y. Lu, R. Eils, B.D. Dynlacht, I. Simon, Genome-wide transcriptional analysis of the human cell cycle identifies genes differentially regulated in normal and cancer cells, Proc. Natl. Acad. Sci. 105 (3) (2008) 955–960, https://doi.org/10.1073/pnas.0704723105.

[44] I. Sheraj, N.T. Guray, S. Banerjee, A pan-cancer transcriptomic study showing tumor specific alterations in central metabolism, Sci. Rep. 11 (1) (2021) 13637, https://doi.org/10.1038/s41598-021-93003-3.

[45] J. Yang, C. Shay, N.F. Saba, Y. Teng, Cancer metabolism and carcinogenesis, Exp. Hematol. Oncol. 13 (1) (2024) 10, https://doi.org/10.1186/s40164-024-00482-x.

[46] X. An, W. Yu, J. Liu, D. Tang, L. Yang, X. Chen, Oxidative cell death in cancer: mechanisms and therapeutic opportunities, Cell Death Dis. 15 (8) (2024) 556, https://doi.org/10.1038/s41419-024-06939-5.

[47] S. Kanno, S. Hirano, T. Mukai, A. Ro, H. Kato, M. Fukuta, Y. Aoki, Cellular uptake of paraquat determines subsequent toxicity including mitochondrial damage in lung epithelial cells, Leg. Med. 37 (2019 Mar) 7–14, https://doi.org/10.1016/j.legalmed.2018.11.008.

[48] C. Fede, C. Millino, B. Pacchioni, B. Celegato, C. Compagnin, P. Martini, F. Selvestrel, F. Mancin, L. Celotti, G. Lanfranchi, M. Mognato, S. Cagnin, Altered Gene Transcription in Human Cells Treated with Ludox® Silica Nanoparticles, Int. J. Environ. Res. Public. Health 11 (9) (2014) 8867–8890. https://doi.org/10.3390/ijerph110908867.

[49] P. Banthia, Rishi Vyas, Ankur Jain, Dhiraj Daga, Takayuki Ichikawa, Vaibhav Kulshrestha, Asha Sharma, R.D. Agarwal, Neha Kapoor, Lokesh Gambhir, Shilpi Gautam, G. Sharma, Biogenic Ag-doped ZnO nanostructures induced cytotoxicity in luminal A and triple-negative human breast cancer cells, Nanomedicine 19 (29) (2024) 2479–2493, https://doi.org/10.1080/17435889.2024.2347825.

[50] M.A. Gatoo, S. Naseem, M.Y. Arfat, A. Mahmood Dar, K. Qasim, S. Zubair, Physicochemical properties of nanomaterials: implication in associated toxic

manifestations, BioMed Res. Int. 2014 (1) (2014) 498420, https://doi.org/10.1155/2014/498420.
[51] P. Xiong, X. Huang, N. Ye, Q. Lu, G. Zhang, S. Peng, H. Wang, Y. Liu, Cytotoxicity of metal-based nanoparticles: from mechanisms and methods of evaluation to pathological manifestations, Adv. Sci. 9 (16) (2022) 2106049, https://doi.org/10.1002/advs.202106049.
[52] Y. Pan, S. Neuss, A. Leifert, M. Fischler, F. Wen, U. Simon, G. Schmid, W. Brandau, W. Jahnen-Dechent, Size-dependent cytotoxicity of gold nanoparticles, Small Weinh. Bergstr. Ger. 3 (11) (2007) 1941–1949, https://doi.org/10.1002/smll.200700378.
[53] A.O. Suliman Y, D. Ali, S. Alarifi, A.H. Harrath, L. Mansour, S.H. Alwasel, Evaluation of cytotoxic, oxidative stress, proinflammatory and genotoxic effect of silver nanoparticles in human lung epithelial cells, Environ. Toxicol. 30 (2) (2015) 149–160, https://doi.org/10.1002/tox.21880.
[54] J.W. Han, S. Gurunathan, J.-K. Jeong, Y.-J. Choi, D.-N. Kwon, J.-K. Park, J.-H. Kim, Oxidative stress mediated cytotoxicity of biologically synthesized silver nanoparticles in human lung epithelial adenocarcinoma cell line, Nanoscale Res. Lett. 9 (1) (2014) 459, https://doi.org/10.1186/1556-276X-9-459.
[55] B.M. Abdallah, E.M. Ali, Therapeutic potential of green synthesized gold nanoparticles using extract of leptadenia hastata against invasive pulmonary aspergillosis, J. Fungi 8 (5) (2022) 442, https://doi.org/10.3390/jof8050442.
[56] C. Uboldi, D. Bonacchi, G. Lorenzi, M.I. Hermanns, C. Pohl, G. Baldi, R.E. Unger, C. J. Kirkpatrick, Gold nanoparticles induce cytotoxicity in the alveolar type-II cell lines A549 and NCIH441, Part. Fibre Toxicol. 6 (1) (2009) 18, https://doi.org/10.1186/1743-8977-6-18.
[57] M. Anandan, H. Gurumallesh Prabu, Dodonaea viscosa leaf extract assisted synthesis of gold nanoparticles: characterization and cytotoxicity against A549 NSCLC cancer cells, J. Inorg. Organomet. Polym. Mater. 28 (3) (2018) 932–941, https://doi.org/10.1007/s10904-018-0799-6.
[58] J. Lebedová, Y.S. Hedberg, I. Odnevall Wallinder, H.L. Karlsson, Size-dependent genotoxicity of silver, gold and platinum nanoparticles studied using the mini-gel comet assay and micronucleus scoring with flow cytometry, Mutagenesis 33 (1) (2018) 77–85, https://doi.org/10.1093/mutage/gex027.
[59] Martínez-Torres AC, Zarate-Triviño DG, Lorenzo-Anota HY, Ávila-Ávila A, Rodríguez-Abrego C, Rodríguez-Padilla C. Chitosan gold nanoparticles induce cell death in HeLa and MCF-7 cells through reactive oxygen species production. Int J Nanomedicine. 2018 May 31;13:3235-3250. doi: 10.2147/IJN.S165289. PMID: 29910612; PMCID: PMC5987788.